Numer. Math. Theor. Meth. Appl.
doi: 10.4208/nmtma.2017.s10

Vol. **10**, No. 2, pp. 420-436
May 2017

Mesh Quality and More Detailed Error Estimates of Finite Element Method

Yunqing Huang*, Liupeng Wang and Nianyu Yi

Hunan Key Laboratory for Computation and Simulation in Science and Engineering, School of Mathematics and Computational Science, Xiangtan University, Xiangtan, Hunan 411105, China

Received 8 November 2016; Accepted (in revised version) 21 January 2017

Dedicated to Professor Zhenhuan Teng on the occasion of his 80th birthday

Abstract. In this paper, we study the role of mesh quality on the accuracy of linear finite element approximation. We derive a more detailed error estimate, which shows explicitly how the shape and size of elements, and symmetry structure of mesh effect on the error of numerical approximation. Two computable parameters G_e and G_v are given to depict the cell geometry property and symmetry structure of the mesh. In compare with the standard a priori error estimates, which only yield information on the asymptotic error behaviour in a global sense, our proposed error estimate considers the effect of local element geometry properties, and is thus more accurate. Under certain conditions, the traditional error estimates and supercovergence results can be derived from the proposed error estimate. Moreover, the estimators G_e and G_v are computable and thus can be used for predicting the variation of errors. Numerical tests are presented to illustrate the performance of the proposed parameters G_e and G_v.

AMS subject classifications: 65N15, 65N30, 65N50

Key words: Finite element methods, error estimation, cell geometry, mesh quality.

1. Introduction

We discuss the role of mesh quality on the accuracy of finite element approximation on triangular meshes. The existing a priori error estimate are in a asymptotic sense

$$\|u - u_h\|_V \leq Ch^m,$$

where V is an appropriate space, C and m are some positive real numbers independ of the mesh size h. The asymptotic estimate shows that the difference between an exact

*Corresponding author. *Email addresses:* huangyq@xtu.edu.cn (Y. Q. Huang), wangliupeng@xtu.edu.cn (L. P. Wang), yinianyu@xtu.edu.cn (N. Y. Yi)

 ©2017 Global-Science Press

https://doi.org/10.4208/nmtma.2017.s10 Published online by Cambridge University Press

solution u and an finite element approximation u_h tends to zero as the mesh size $h \to 0$. In general, it is a very difficult task to explicitly evalute how the constant C depends on the mesh quality. To our best knowledge, the role of the cell gemoetry and mesh quality on the accuracy of approximation is not widely addressed in the literature. Some discussion of this topic can be found in [1, 19]. In [16], Yi and Huang established a fundamental error estimation on general mesh, and designed a computable parameter to depict the role of mesh quality on the accuracy of finite element approximation.

The standard a priori error estimate is often insufficient since: i) it only yield information on the asymptotic error behaviour, and is useless for the adaptive meshes with local refinement; ii) the value of the constant C depends on the exact solution u and can be very large on a mesh with "bad" cell geometry; iii) the value of the constant C also can be infinitesimal on a mesh with higher quality. To make the estimate more accurately, an obvious remedy is to refine the estimation by considering how the C depends on finite element mesh. The question then is how to discribe the mesh quality's effect on the accuracy of finite element approximation and how to quantify the approximation error on a mesh with element size vary greatly. These considerations clearly show the need for an estimation which can show the role of the cell geometry and mesh quality on the accuracy of finite element approximation. Of course, the derived error estimation should be localized and should show explicitly how the constant C depends on the shape and size of elements. Moreover, the calculation of the error estimator can be a priori extracted from the cell geometry and mesh quality.

The objective of this paper is to study the role of cell geometry and the symmetry structure of mesh on the accuracy of finite element method. We discuss how the accuracy of finite element approximation depends on the cell geometry and the mesh structure. In detail, we proposed the following error estimations:

$$\begin{aligned}
&\|\nabla(u_I - u_h)\| \lesssim G_e + G_v + h.o.t,\\
&\|u - u_h\|_{\ell^2} \lesssim G_v + h.o.t,
\end{aligned}$$

where u_h is the fintie element approximation and u_I is the piecewise linear interpolant of u, h.o.t denotes the higher order terms, and G_e and G_v are defined as follows:

$$G_e = \left(\sum_{e\in\mathcal{E}} |\omega_e| \ell_k^2 \left([\theta_{k+1}]^2 + [\theta_{k-1}]^2 + \left[\frac{\ell_{k+1}}{\ell_k}\right]^2 + \left[\frac{\ell_{k-1}}{\ell_k}\right]^2 \right) \left(1 - \frac{Q_\tau + Q_{\tau'}}{2}\right) \right)^{1/2},$$

$$G_v = \left(\sum_{\tau\in\mathcal{T}_h} |\tau| (\ell_k^2 + \ell_{k-1}^2 + \ell_{k+1}^2)^2 (1 - Q_\tau) \right)^{1/2}.$$

The details are stated in Section 2. The error estimations show explicitly how the errors depend on the shape and size of elements, and symmetry of the mesh. The two computable parameters G_e and G_v are proposed for depicting the cell geometry and symmetry structure of the mesh. As a by-product, we are easy to obtain various known superconvergence results based on the presented parameters.

https://doi.org/10.4208/nmtma.2017.s10 Published online by Cambridge University Press

The organization of the paper is as follows. In Section 2, we report the main results, and present the corresponding numerical tests for illustrating the reliability and efficiency of the designed parameters. As a result of our analysis, we discuss the superconvergence on centroidal Voronoi-Delaunay triangulation in Section 3. The approach is illustrated by numerical tests. Finally, concluding remarks and comments for future work are provided in Section 4.

2. Main observations

In this section, we carefully investigate how the accuracy of finite element approximation depends on the element geometry and the mesh structure with Poisson equation solved by linear triangular elements. We consider the following model problem:

$$\begin{cases} -\Delta u = f & \text{in } \Omega, \\ u = g & \text{on } \partial\Omega, \end{cases} \tag{2.1}$$

where $\Omega \subset \mathcal{R}^2$ is a bounded domain with Lipschitz boundary $\partial\Omega$.

In weak form, this problem reads: Find $u \in H_g^1(\Omega) := \{v \in H^1(\Omega) | v|_{\partial\Omega} = g\}$ such that

$$a(u, v) = (f, v), \quad \forall v \in H_0^1(\Omega), \tag{2.2}$$

where

$$a(u, v) = \int_\Omega \nabla u \cdot \nabla v dx,$$

and $(\cdot, \cdot)$ denotes the inner product of $L^2(\Omega)$.

Let $\mathcal{T}_h$ be a shape regular triangulation of Ω and V_h be the linear finite element space over $\mathcal{T}_h$ defined by

$$V_h = \{v \in C^0(\Omega) : v|_\tau \in P_1(\tau),\ \forall \tau \in \mathcal{T}_h; v(x, y) = g(x, y),\ \forall (x, y) \in \mathcal{N}_\Gamma\},$$
$$V_h^0 = \{v \in C^0(\Omega) : v|_\tau \in P_1(\tau),\ \forall \tau \in \mathcal{T}_h; v(x, y) = 0,\ \forall (x, y) \in \mathcal{N}_\Gamma\},$$

where $\mathcal{N}_\Gamma$ denotes the mesh nodes on the domain boundary $\partial\Omega$, and $P_k(D)$ denotes the set polynomials defined in $D \in \mathbb{R}^2$ of total degree no more than k. The finite element solution of (2.2) is to find $u_h \in V_h$ such that

$$a(u_h, v) = (f, v), \quad \forall v \in V_h^0. \tag{2.3}$$

For a canonical element τ. Let τ have vertices (x_k, y_k), $1 \le k \le 3$, oriented counterclockwise, and corresponding nodal basis functions $\{\lambda_k\}_{k=1}^3$. Let $\{e_k\}_{k=1}^3$ denote the edges of element τ, $\{\theta_k\}_{k=1}^3$ the angles, $\{\boldsymbol{n}_k\}_{k=1}^3$ the unit outward normal vectors, $\{\boldsymbol{t}_k\}_{k=1}^3$ the unit tangent vectors with counterclockwise orientation, $\{\ell_k\}_{k=1}^3$ the edge lengths, and $\{d_k\}_{k=1}^3$ the prependicular heights.

For a given triangulation $\mathcal{T}_h$, let h denote the mesh size, and $h_\tau := diam(\tau)$ for each $\tau \in \mathcal{T}_h$. Let $\mathcal{E}$ denote the set of interior edges in $\mathcal{T}_h$, for $e \in \mathcal{E}$, h_e denote the length of

https://doi.org/10.4208/nmtma.2017.s10 Published online by Cambridge University Press

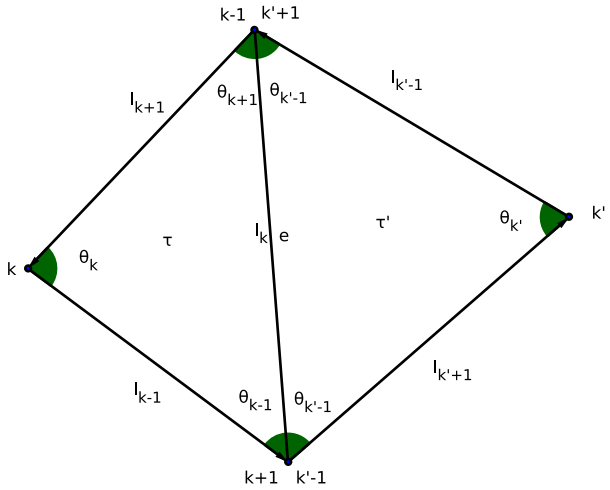


Figure 1: Parameters associated with the interior edge e.

e, and $\omega_e = \tau \cup \tau'$ with τ and τ' be the two elements sharing e. For any triangle $\tau \in \mathcal{T}_h$, let element quality be defined as

$$Q_\tau := \frac{4\sqrt{3}|\tau|}{\ell_1^2 + \ell_2^2 + \ell_3^2}.$$

We now defined two quantities which are used for quantifying the effect of the mesh quality on the accuracy of finite element approximation.

$$G_e = \left(\sum_{e \in \mathcal{E}} |\omega_e| \ell_k^2 \left([\theta_{k+1}]^2 + [\theta_{k-1}]^2 + \left[\frac{\ell_{k+1}}{\ell_k} \right]^2 + \left[\frac{\ell_{k-1}}{\ell_k} \right]^2 \right) \left(1 - \frac{Q_\tau + Q_{\tau'}}{2} \right) \right)^{\frac{1}{2}}, \tag{2.4}$$

and

$$G_v = \left(\sum_{\tau \in \mathcal{T}_h} |\tau| (\ell_k^2 + \ell_{k-1}^2 + \ell_{k+1}^2)^2 (1 - Q_\tau) \right)^{1/2}, \tag{2.5}$$

where $[w]_e = w|_{e^+} - w|_{e^-}$ denotes the jump of w at the edge e. We then state our main observations as follows:

Main observations: Assume that the solution u is sufficiently regular. For any shape regular triangulation $\mathcal{T}_h$, we have

$$\|\nabla(u_I - u_h)\| \lesssim G_e + G_v + h.o.t, \tag{2.6a}$$

$$\|u - u_h\|_{\ell^2} \lesssim G_v + h.o.t, \tag{2.6b}$$

where h.o.t denotes the higher order termes in compare with G_e and G_v as $h \to 0$, and

$$\|u - u_h\|_{\ell^2} := \left(\frac{1}{N} \sum_{k=1}^{N} |(u - u_h)(x_k, y_k)|^2 \right)^{1/2}$$

https://doi.org/10.4208/nmtma.2017.s10 Published online by Cambridge University Press

with N denotes the number of nodes in mesh $\mathcal{T}_h$.

For a given mesh, the two proposed parameters G_e and G_v in (2.4)-(2.5) are computable and can be used to indicate how the accuracy of finite element approximation depends on the element geometry and the mesh structure. Moreover, one can predict the errors of finite element approximation by evaluating G_e and G_v.

In the following, we present some numerical examples to demonstrate the performance of the parameters G_e and G_v.

Experiment 2.1. In our first experiment, we consider the Poisson equation on the square domain with the exact solution $u = e^{x+y}$. The errors and the data G_e and G_v are ploted in Fig. 2. It is quite clearly that:

(i) For the uniform mesh in regular pattern, $G_e = 0$, and

$$G_v = \mathcal{O}(N^{-1}), \quad \|\nabla(u_I - u_h)\| = \mathcal{O}(N^{-1}), \quad \|u - u_h\|_{\ell^2} = \mathcal{O}(N^{-1}).$$

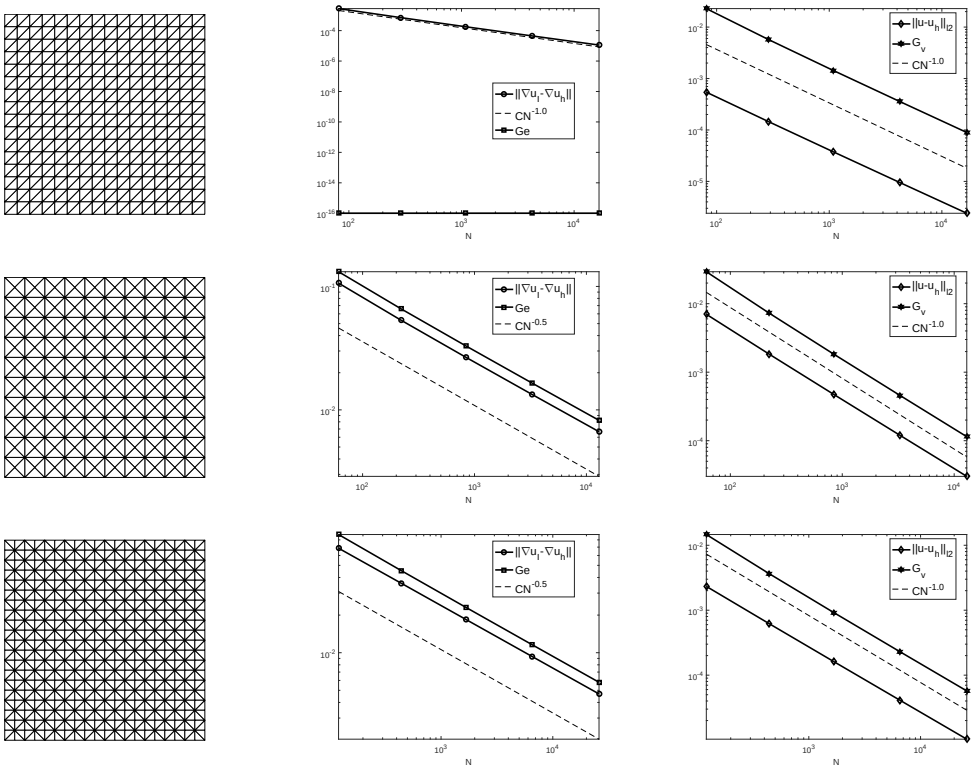


Figure 2: Experiment 2.1: square domain, uniform mesh. From left to right are the mesh, error $\|\nabla(u_h - u_I)\|$ and G_e, error $\|u - u_h\|_{\ell^2}$ and G_v. Top: results on regular pattern, Middle: results on Criss-Cross pattern, Down: results on Union-Jack pattern.

https://doi.org/10.4208/nmtma.2017.s10 Published online by Cambridge University Press

(ii) For the uniform mesh in criss-cross pattern and union-jack pattern,

$$G_e = \mathcal{O}(N^{-1/2}), \qquad G_v = \mathcal{O}(N^{-1}),$$
$$\|\nabla(u_I - u_h)\| = \mathcal{O}(N^{-1/2}), \qquad \|u - u_h\|_{\ell^2} = \mathcal{O}(N^{-1}).$$

The parameters G_e and G_v are reliable and efficient for estimating errors $\|\nabla(u_I - u_h)\|$ and $\|u - u_h\|_{\ell^2}$. The convergence rates of G_e and G_v can indicate the convergence rates of $\|\nabla(u_I - u_h)\|$ and $\|u - u_h\|_{\ell^2}$. This confirms the results in (2.6). Thus, we can determine the rates of error $\|\nabla(u_I - u_h)\|$ and $\|u - u_h\|_{\ell^2}$ by evaluating G_e and G_v.

Experiment 2.2. To test the robust of the two proposed parameters G_e and G_v in estimation (2.6), we solving (2.1) on different type of meshes with similar mesh nodes. The meshes and the corresponding errors and data are shown in Figs. 3-4. We can see that:

(i) For different type meshes, the accuracy of the finite approximation are different. This shows that the accuracy is sensitive to the cell geometry and mesh structure.

(ii) The changing trends of G_e and G_v are coincide with the trends of errors $\|\nabla(u_h - u_I)\|$ and $\|u - u_h\|_{\ell^2}$, respectively. Thus the proposed two parameters can well describle the role of mesh quality on accuracy of finite element approximation.

Experiment 2.3. In our third experiment, we solve (2.1) on a sequence of meshes which are generated in the procedure of mesh optimization algorithm. The initial mesh is randomly generated. We applying the linear finite element method on the mesh generated by each optimization step. The sampled meshes and the history of the data and errors are ploted in Figs. 5-6. We clearly see that the mesh quality is increase in the process of mesh optimization, and the errors $\|\nabla(u_h - u_I)\|$ and $\|u - u_h\|_{\ell^2}$ are decrease, also the parameters G_e and G_v are in good agreement with the errors $\|\nabla(u_h - u_I)\|$ and $\|u - u_h\|_{\ell^2}$, respectively.

Experiment 2.4. Finally, we test the performance of the parameters G_e and G_v in the adaptive meshes. We consider the Poisson equation on the L-shape domain $\Omega = (-1,1)^2 \setminus [0,1) \times (-1,0]$ with $f = 0$ and the Dirichlet boundary condition, using a polar coordinate system, the exact solution is

$$u = r^{2/3} \sin\left(\frac{2}{3}\theta\right).$$

The true solution has singularity at the point $(0,0)$. We using the centroidal Voronoi tessellation (CVT) based refine methods [7] for mesh adaption. The adaptive meshes and corresponding data are plotted in Fig. 7. We see clearly that,

$$\|\nabla(u_h - u_I)\| \approx G_e = \mathcal{O}(N^{-0.7}), \quad \|u - u_h\|_{\ell^2} \approx G_v = \mathcal{O}(N^{-1.1}).$$

The convergence rate of G_e and $\|\nabla(u_h - u_I)\|$, G_v and $\|u - u_h\|_{\ell^2}$ are well matched on the CVT refined meshes. This shows that the parameters G_e and G_v also reliable and efficient in the adaptive procedure.

https://doi.org/10.4208/nmtma.2017.s10 Published online by Cambridge University Press

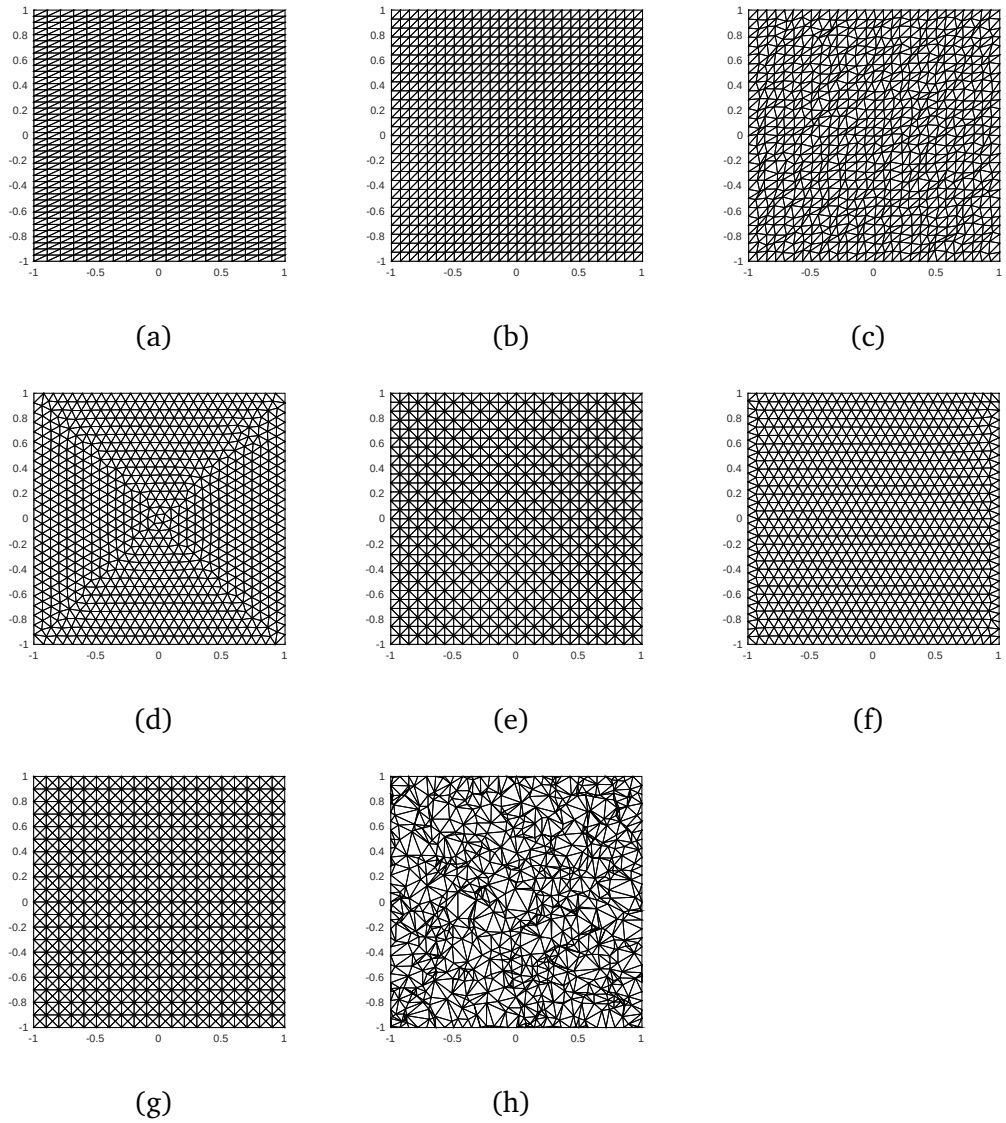


Figure 3: Experiment 2.2: square domain. (a) Regular mesh with 20 and 42 nodes in x and y direction, respectively; (b) Regular mesh; (c) Regular mesh with small perturbation; (d) CVDT mesh; (e) Union-Jack mesh; (f) Mesh generated by DistMesh [14]; (g) Criss-Cross mesh; (h) Mesh generated by randomly.

3. Application to superconvergence

Superconvergence techniques are very important numerical tools to achieve high accuracy finite element approximations, see [2–4, 8–11, 17, 20] and the monographs by Chen and Huang [5], Wahlbin [15], Lin and Yan [13], Zhu and Lin [18] and a review article by Lakhany, Marek, and Whiteman [12]. In recent years, there is a revitalization of the research of this subject because of its relevance with a posteriori error estimations

https://doi.org/10.4208/nmtma.2017.s10 Published online by Cambridge University Press

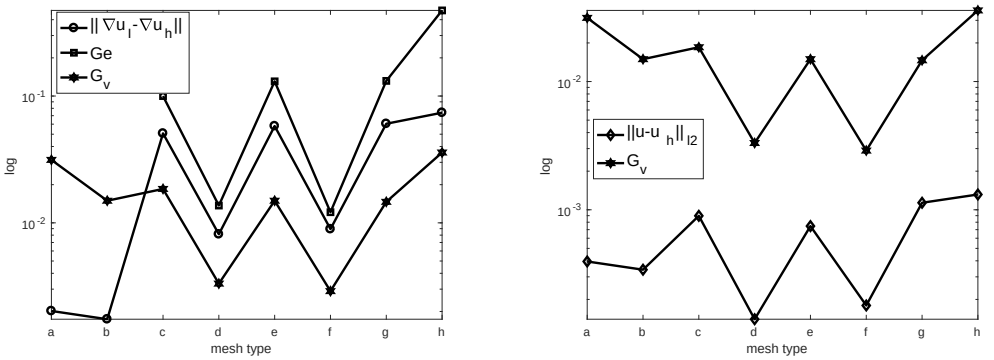


Figure 4: Experiment 2.2, left: error $\|\nabla(u_h - u_I)\|$ and data G_e, G_v; right: error $\|u - u_h\|_{\ell^2}$ and data G_v, the corresponding meshes are shown in Fig. 3.

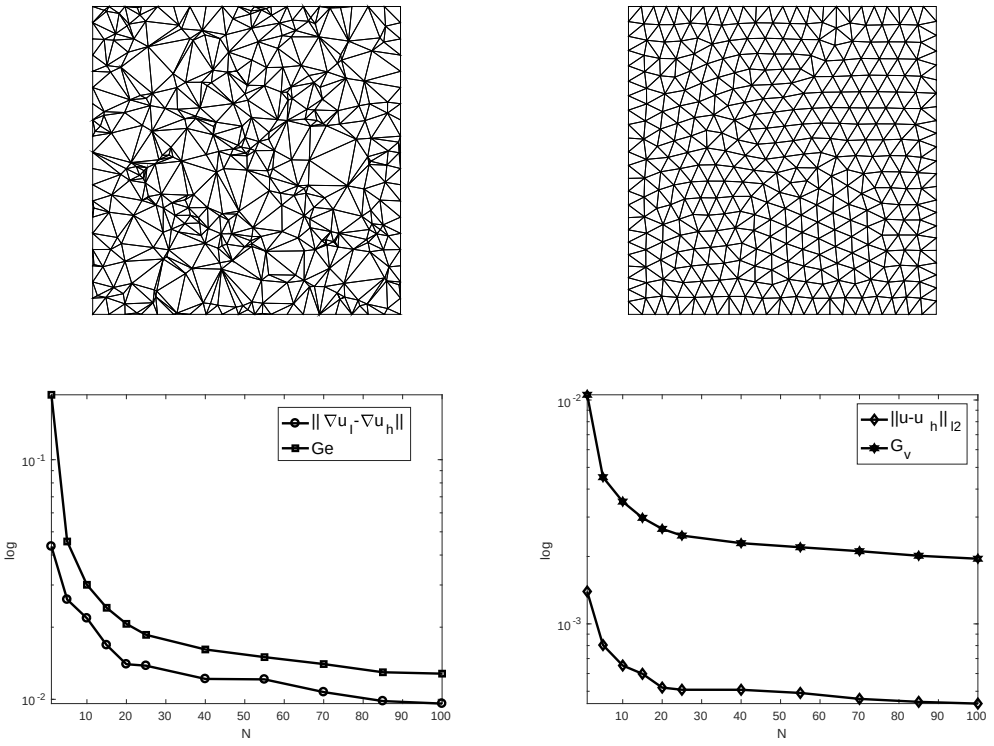


Figure 5: Experiment 2.3: square domain, meshes, the data G_e, G_v, and errors $\|\nabla(u_h - u_I)\|$, $\|u - u_h\|_{\ell^2}$. Left top: inital mesh, randomly generated, Right top: optimizated with 100 steps, Left down: history of data G_e and errror $\|\nabla(u_h - u_I)\|$, Right down: history of data G_v and errror $\|u - u_h\|_{\ell^2}$.

for finite element grid adaptation. The superconvergence of the finite element method is senstive to the quality of mesh. The existing superconvergence results usually require the mesh satisfy some strong conditions, such as uniform mesh, strongly regular mesh or mildly structured mesh, while locally refinement would break the symmetry

https://doi.org/10.4208/nmtma.2017.s10 Published online by Cambridge University Press

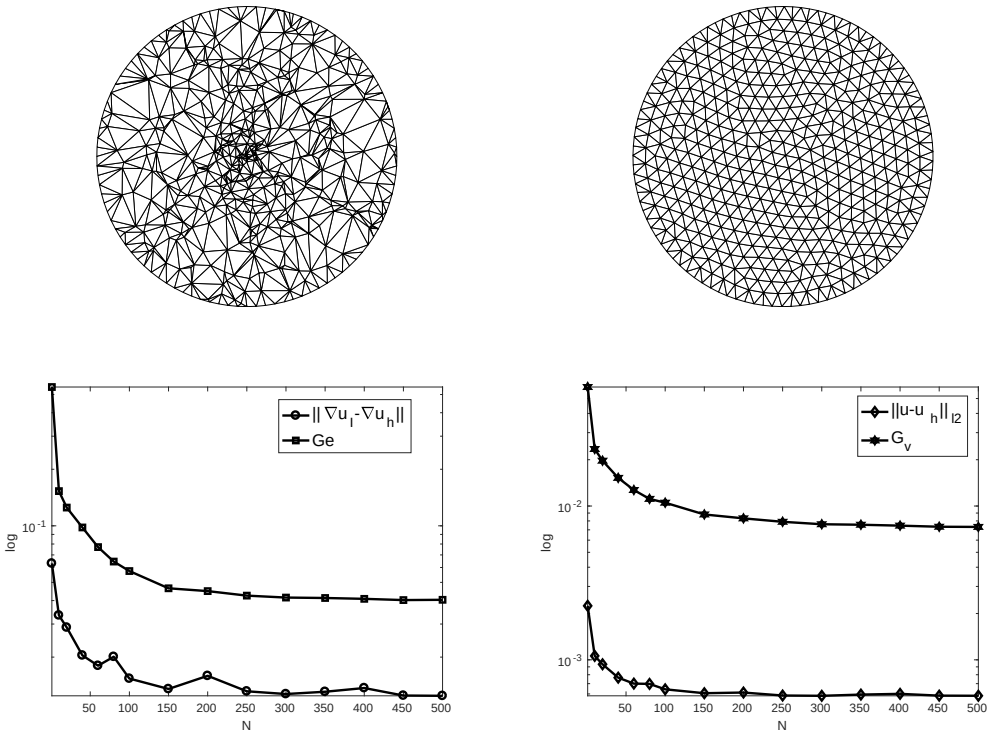


Figure 6: Experiment 2.3: unit disk domain, meshes, the data G_e, G_v, and errors $\|\nabla(u_h - u_I)\|$, $\|u - u_h\|_{\ell^2}$. Left top: inital mesh, randomly generated, Right top: optimizated with 500 steps, Left down: history of data G_e and errror $\|\nabla(u_h - u_I)\|$, Right down: history of data G_v and errror $\|u - u_h\|_{\ell^2}$.

structure of the mesh. To promote the application of superconvergence techniques in adaptive computations, it is quite necessary to study the role of mesh quality on the superconvergence. More precisely, a parameter should be introduced to measure the symmetry sturcture of a given mesh, then one can varify the superconvergence phenomenon by evaluating the parameter.

Based on the error estimation presented in (2.6), we are now ready to present various known superconvergence results on some type of triangular meshes which are used in finite element methods widely. We will first recovery various known results and finally will present our result on the meshes generated by centroidal Voronoi tessellation.

Globally uniform mesh. Let us first take a look at a simple case that the triangulation $\mathcal{T}_h$ is uniform, namely every two adjacent triangles τ and τ' forms a perfect parallelogram. From the basic error expansions, we obtain

Corollary 3.1. *If the triangulation $\mathcal{T}_h$ is uniform, then*

$$G_e = 0, \quad G_v = \mathcal{O}(h^2), \tag{3.1}$$

and

$$\|\nabla(u_I - u_h)\| \leq Ch^2, \quad \|u - u_h\|_{\ell^2} \leq Ch^2. \tag{3.2}$$

https://doi.org/10.4208/nmtma.2017.s10 Published online by Cambridge University Press

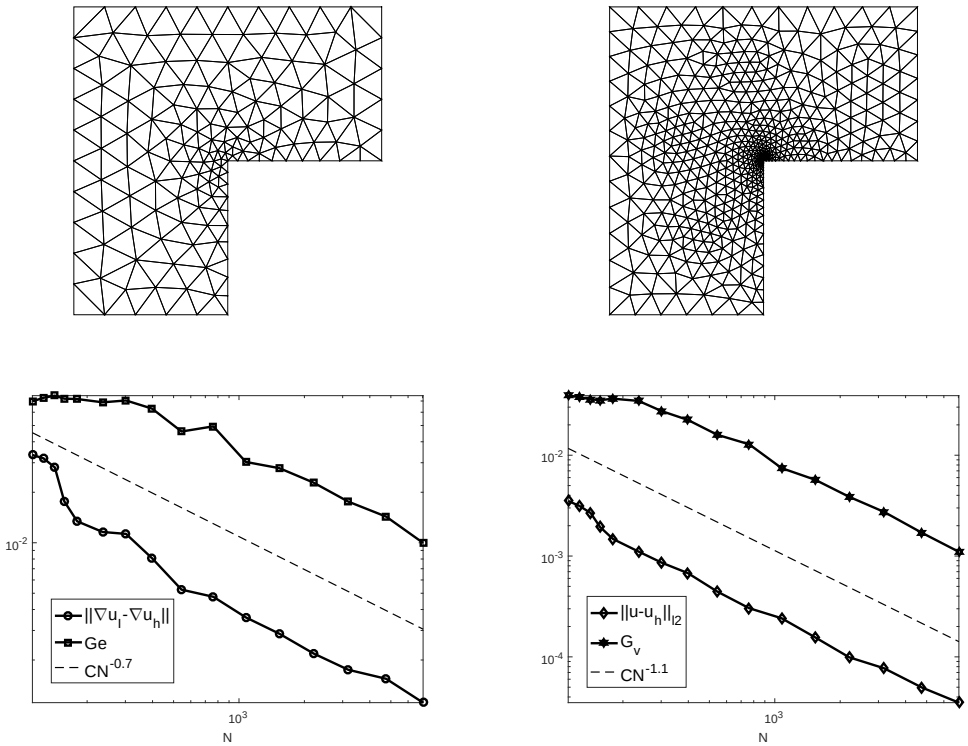


Figure 7: Experiment 2.4: L-shape domain, adaptive mesh using CVT refinement, the convergence rates of parameters G_e, G_v, and erors $\|\nabla(u_h - u_I)\|$, $\|u - u_h\|_{\ell^2}$. Left top: mesh after 5 refinements, Right top: mesh after 10 refinements, Left down: history of error $\|\nabla(u_h - u_I)\|$, Right down: history of error $\|u - u_h\|_{\ell^2}$.

Proof. As triangulation $\mathcal{T}_h$ is uniform, then $G_e = 0$, $Q_\tau \equiv \frac{\sqrt{3}}{2}$, and

$$G_v = \left(\frac{2-\sqrt{3}}{2} \sum_{\tau \in \mathcal{T}_h} |\tau| (\ell_k^2 + \ell_{k-1}^2 + \ell_{k+1}^2)^2 \right)^{1/2} = \mathcal{O}(h^2).$$

Then (3.2) follows from (2.6). □

Strongly regular mesh. Classic superconvergence results are often obtained for the so-called strongly regular mesh is such that if any two adjacent triangles form an $\mathcal{O}(h^2)$ approximate parallelogram. Similarly, we have the superconvergence results for globally strongly regular mesh.

Corollary 3.2. *If the triangulation $\mathcal{T}_h$ is strongly regular, then*

$$G_e = \mathcal{O}(h^2), \quad G_v = \mathcal{O}(h^2), \tag{3.3}$$

and

$$\|\nabla(u_I - u_h)\| \le Ch^2, \qquad \|u - u_h\|_{\ell^2} \le Ch^2. \tag{3.4}$$

https://doi.org/10.4208/nmtma.2017.s10 Published online by Cambridge University Press

Proof. Since the triangulation $\mathcal{T}_h$ is strongly regular, for any interior edge e, we have

$$\ell_{k+1} - \ell_{k'+1} = \mathcal{O}(h^2), \quad \ell_{k-1} - \ell_{k'-1} = \mathcal{O}(h^2).$$

Then

$$\theta_{k+1} - \theta_{k'+1} = \mathcal{O}(h), \quad \theta_{k-1} - \theta_{k'-1} = \mathcal{O}(h),$$

and

$$0 < Q_\tau \leq 1, \quad 0 \leq 1 - Q_\tau < 1.$$

Thus

$$G_e \leq Ch^2, \quad G_v \leq Ch^2,$$

and estimation (3.4) can be obtained from (2.6) immediately. □

Mildly structured mesh. In practical computations, triangulation obtained by most mesh generators can not be completely unstructured. In most practical grids, most pairs of triangles form an approximate parallelogram although the entire grid is not strongly regular. We show the similar superconvergence result on this type of mesh.

Corollary 3.3. *If the triangulation $\mathcal{T}_h$ satisfies the following properties: let $\mathcal{E} = \mathcal{E}_1 \bigoplus \mathcal{E}_2$ denote the set of interior edges in $\mathcal{T}_h$, for each $e \in \mathcal{E}_1$, the adjacent τ and τ' form an $\mathcal{O}(h^2)$ approximate parallelogram, while*

$$\sum_{e \in \mathcal{E}_2} |\tau| + |\tau'| = \mathcal{O}(h^{2\sigma}).$$

Then

$$G_e = \mathcal{O}(h^{1+\min\{1,\sigma\}}), \quad G_v = \mathcal{O}(h^2), \tag{3.5}$$

and

$$\|\nabla(u_I - u_h)\| \leq Ch^{1+\min\{1,\sigma\}}, \quad \|u - u_h\|_{\ell^2} \leq Ch^2. \tag{3.6}$$

Proof. Easily, we get

$$\begin{aligned}
&|\theta_{e+1} - \theta_{e'+1}| + |\theta_{e-1} - \theta_{e'-1}| = \mathcal{O}(h), && \forall e \in \mathcal{E}_1,\\
&|\theta_{e+1} - \theta_{e'+1}| + |\theta_{e-1} - \theta_{e'-1}| = \mathcal{O}(1), && \forall e \in \mathcal{E}_2,\\
&0 < Q_\tau \leq 1, \qquad 0 \leq 1 - Q_\tau < 1.
\end{aligned}$$

Then

$$G_e = \mathcal{O}(h^{1+\min\{1,\sigma\}}), \quad G_v = \mathcal{O}(h^2).$$

From (2.6), we immediately obtain (3.6). □

Centroidal Voronoi-Delaunay triangulation. We now consider the superconvergence on centroidal Voronoi-Delaunay triangulation (CVDT) mesh. The CVT [6] often provide

https://doi.org/10.4208/nmtma.2017.s10 Published online by Cambridge University Press

optimal point distributions, thus making CVT based mesh generation and optimization techniques very effictive. The dual Delaunay triangulation is called the CVDT which often yields high-quality Delaunay meshes. The basis Voronoi cell of the CVT was shown to be the regular hexagon in two dimension, and then its dual Delaunay triangulation approaches a equilateral triangle mesh except some pieces. Huang, Qin and Wang [7] have shown that there is superconvergence phenomena on the mesh based on CVDT for Poisson problem from numerical investigation. We using the following definitions to measure the mesh quality. Let

$$Q = \frac{1}{M}\sum_{i=1}^{M} Q_{\tau_i}, \quad Q_{\tau_i} = \frac{4\sqrt{3}|\tau_i|}{\ell_1^2+\ell_2^2+\ell_3^2}.$$

Obviously, the bigger of Q, the better of the mesh. For the CVDT, the mesh quality

$$Q \to 1 \ \text{ as } \ h \to 0.$$

In the following, we first numerical investigate the convergence rates of $Q \to 1$. Then we derive the superconvergence results for CVDT based on the numerical observation.

As the triangulation $\mathcal{T}_h$ generated by CVDT approaches a equilateral triangle mesh except some pieces, one can expect that the quantity $1-Q$ converge to 0 with a rate $\gamma > 0$. To verify this property, some numerical tests have done. The results are shown in Fig. 8. It shows that

$$1 - Q = \mathcal{O}(h^{\gamma}), \quad \gamma \approx 1.0.$$

The relationship between G_v and $1-Q$ is:

$$\begin{aligned} G_v = &\left(\sum_{\tau\in\mathcal{T}_h} |\tau|(\ell_k^2+\ell_{k-1}^2+\ell_{k+1}^2)^2\,(1-Q_\tau)\right)^{1/2} \le C\left(\sum_{\tau\in\mathcal{T}_h} h^6(1-Q_\tau)\right)^{1/2} \\ \le & Ch^2\left(1-N^{-1}\sum_{\tau\in\mathcal{T}_h} Q_\tau)\right)^{1/2} \le Ch^2\,(1-Q)^{1/2}\,. \end{aligned}$$

Thus the convergence rate of G_v is approximately $2+\frac{\gamma}{2}$.

From the numerical investigation, we see that, if the triangulation $\mathcal{T}_h$ generated by CVDT, the convergence rates of G_e and G_v satisfy

$$G_e = \mathcal{O}(h^{1+\gamma/2}), \quad G_v = \mathcal{O}(h^{2+\gamma/2}), \quad \gamma > 0. \tag{3.7}$$

Then, in practical, we can use G_e and G_v to depict the cell geometry and symmetry of the mesh and help us to verify the superconvergence phenomenon.

Combining with estimation (2.6), we obtain the following superconvergence result for CVDT mesh.

https://doi.org/10.4208/nmtma.2017.s10 Published online by Cambridge University Press

Corollary 3.4. *Let the triangulation $\mathcal{T}_h$ generated by CVDT, and assume that the mesh parameters G_e and G_v satisfy* (3.7). *Let u and u_h be the solution of* (2.2) *and* (2.3), *respectively, and u_I be the continuous piecewise linear interpolant of u. Then*

$$\|\nabla(u_I - u_h)\| \leq Ch^{1+\gamma/2}, \quad \|u - u_h\|_{\ell^2} \leq Ch^{2+\gamma/2}. \tag{3.8}$$

Experiment 3.1. In the following, we present some numerical tests to demonstrate the performance of the parameters G_e and G_v on CVDT mesh. We consider the model problem (2.1) with $u = e^{x+y}$. We carry out our numerical experiments on different domains including the square domain, disk domain, and also some complicated domains, which are shown in Fig. 8. Figs. 9-13 plot the data G_e, G_v and the errors $\|\nabla(u_h - u_I)\|$,

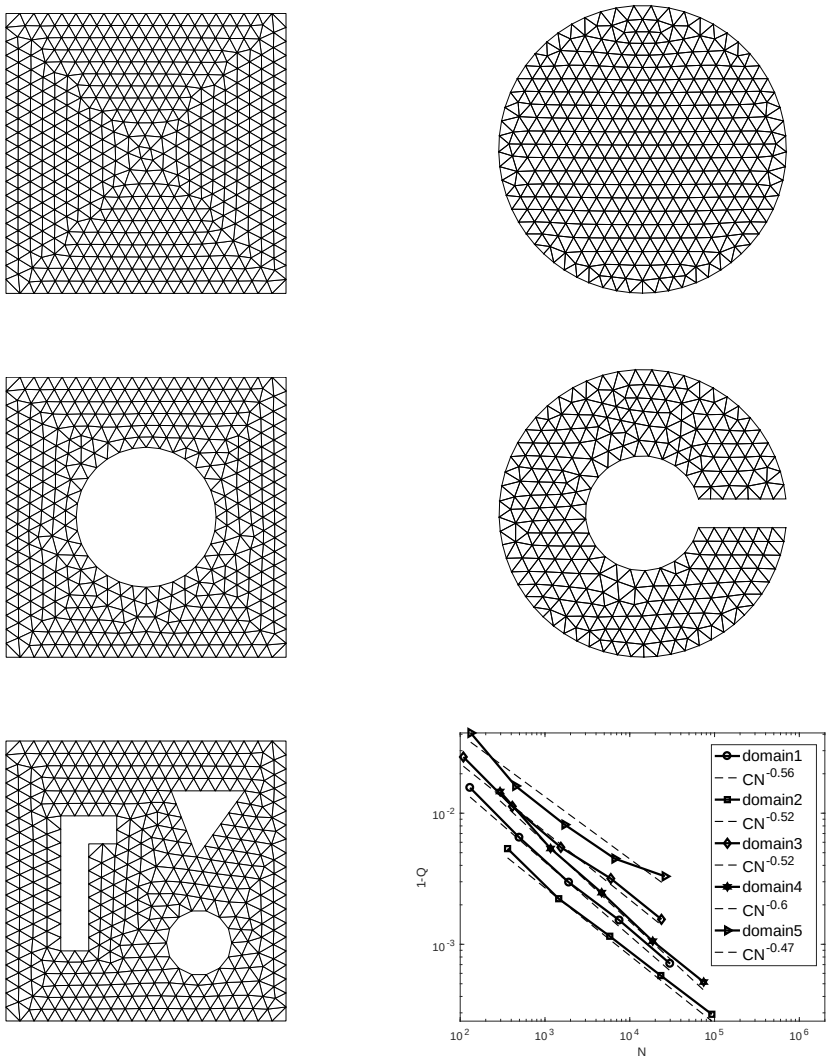


Figure 8: The convergence rates of $1 - Q$ for different domain. Left top: domain 1; Right top: domain 2; Left middle: domain 3; Right middle: domain 4; Left down: domain 5; Right down: history of $1 - Q$.

https://doi.org/10.4208/nmtma.2017.s10 Published online by Cambridge University Press

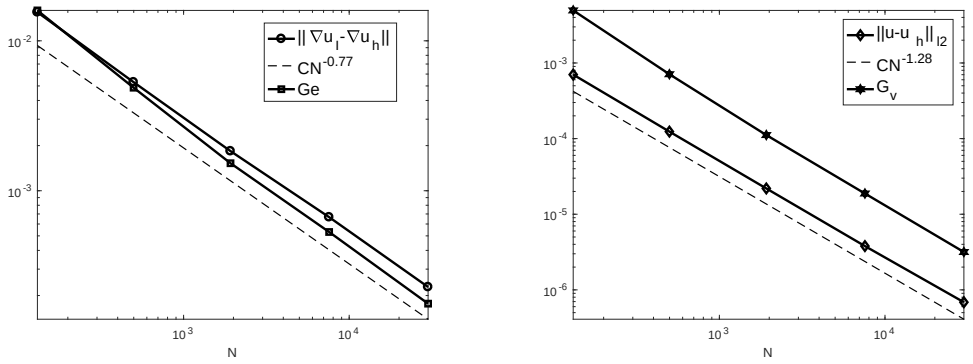


Figure 9: Experiment 3.1: domain 1 in Fig. 8, the convergence rates of parameters G_e, G_v, and erors $\|\nabla(u_h - u_I)\|$, $\|u - u_h\|_{\ell^2}$.

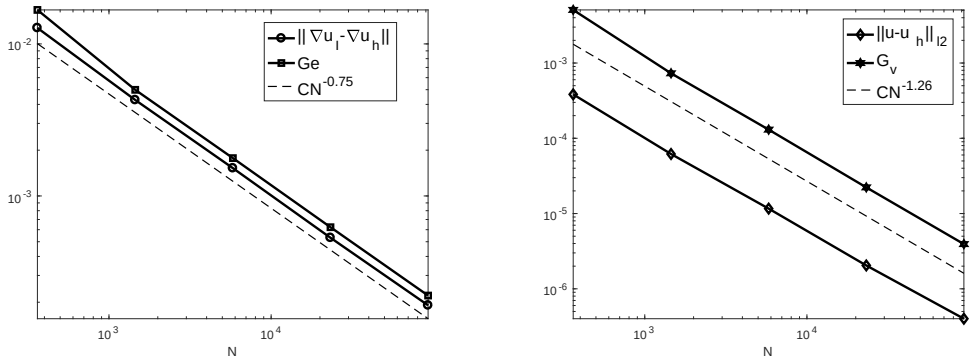


Figure 10: Experiment 3.1: domain 2 in Fig. 8, the convergence rates of parameters G_e, G_v, and erors $\|\nabla(u_h - u_I)\|$, $\|u - u_h\|_{\ell^2}$.

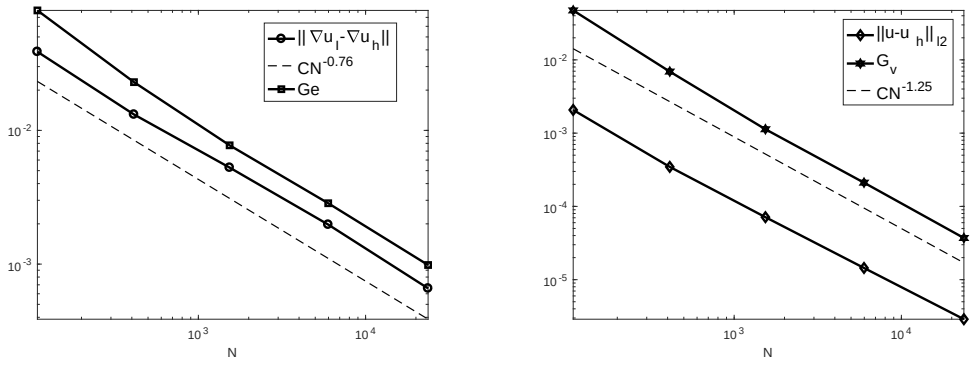


Figure 11: Experiment 3.1: domain 3 in Fig. 8, the convergence rates of parameters G_e, G_v, and erors $\|\nabla(u_h - u_I)\|$, $\|u - u_h\|_{\ell^2}$.

$\|u - u_h\|_{\ell^2}$, respectively. It is quite clearly that

$$G_e = O(N^{-(1/2+\gamma/4)}), \quad G_v = \mathcal{O}(N^{-(1+\gamma/4)}), \quad \gamma \approx 1.0,$$
$$\|\nabla(u_h - u_I)\| \approx C(G_e + G_v) = \mathcal{O}(N^{-(1/2+\gamma/4)}),$$
$$\|u - u_h\|_{\ell^2} \approx CG_v = \mathcal{O}(N^{-(1+\gamma/4)}).$$

https://doi.org/10.4208/nmtma.2017.s10 Published online by Cambridge University Press

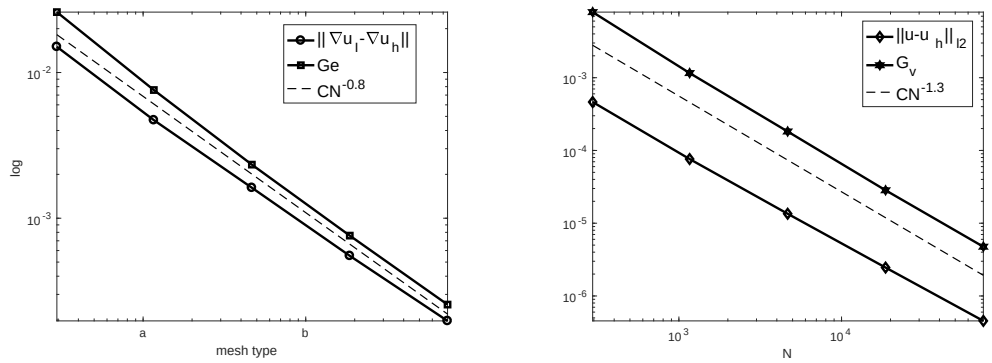


Figure 12: Experiment 3.1: domain 4 in Fig. 8, the convergence rates of parameters G_e, G_v, and erors $\|\nabla(u_h - u_I)\|$, $\|u - u_h\|_{\ell^2}$.

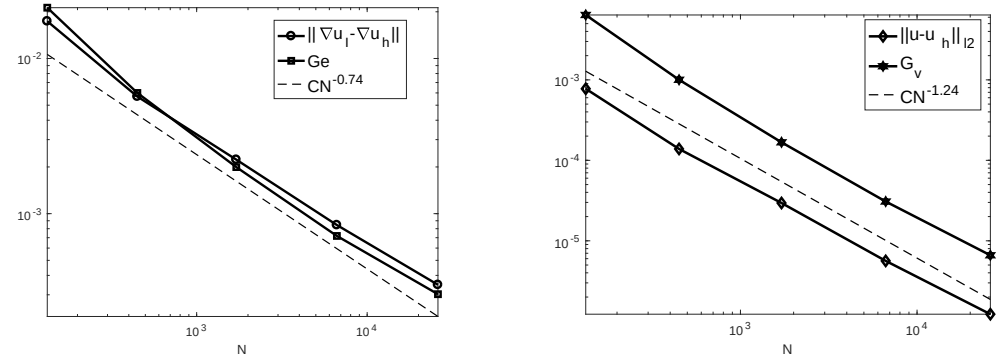


Figure 13: Experiment 3.1: domain 5 in Fig. 8, the convergence rates of parameters G_e, G_v, and erors $\|\nabla(u_h - u_I)\|$, $\|u - u_h\|_{\ell^2}$.

This confirms that the proposed parameters G_e and G_v can exactly indicate the superconvergence property of the CVTD mesh.

4. Concluding remarks and future work

We have proposed two computable parameters G_e, G_v to depict the cell geometry and symmetry structure of a mesh. In compare with the standard error estimates, which are in a asymptotic behaviour and globally, our error estimation is more accuracy since its show explicitly how the errors depend on the shape and size of elements, and symmetry of mesh. By evaluating G_e and G_v, we can verify whether the finite element solution u_h is superclose to the interpolant u_I, and the superconvergence of the finite approximation on the mesh nodes. These results can be applied in the a posteriori error estimation and adaptive finite element methods. We will report these applications in our future work.

https://doi.org/10.4208/nmtma.2017.s10 Published online by Cambridge University Press

Acknowledgments Huang's research was partially supported by NSFC Project (No. 91430213). Wang's research was supported by Hunan Provincial Innovation Foundation for Postgraduate (No. CX2015 B209) and NSFC Project (No. 11301449). Yi's research was partially supported by NSFC Project (No. 11671341), Hunan Provincial NSF Project (No. 2015JJ2145) and Hunan Education Department Project (No. 16A206).

References

[1] I. BABUSKA AND A. AZIZ, *On the angle condition in the finite element method*, SIAM J. Numer. Anal., 13 (1976), pp. 214–226.
[2] C. CHEN, *Optimal points of the stresses for triangular linear element*, Numer. Math. J. Chinese Univ., 2 (1980), pp. 12–20(in Chinese).
[3] C. CHEN, *Superconvergence of finite element solutions and their derivatives*, Numer. Math. J. Chinese Univ., 3 (1981), pp. 118–125(in Chinese).
[4] C. CHEN, *Superconvergence of finite element approximations to nonlinear elliptic problems*, (Proc. China-France Sympos. on Finite Element Methods, Beijing, 1982), Gordon and Breach, New York, pp. 622–640, 1983.
[5] C. CHEN AND Y. HUANG, High Accuracy Theory of Finite Element Methods, Hunan Science Press, Hunan, China(in Chinese), 1995.
[6] Q. DU, V. FABER AND M. GUNZBURGER, *Centroidal Voronoi tessellations: applications and algorithms*, SIAM Rev., 41 (1999), pp. 637–676.
[7] Y. HUANG, H. QIN AND D. WANG, *Centroidal Voronoi tessellation-based finite element superconvergence*, Int. J. Numer. Methods Eng., 76 (2008), pp. 1819–1839.
[8] Y. HUANG, J. LI, C. WU AND W. YANG, *Superconvergence analysis for linear tetrahedral edge elements*, J. Sci. Comput., 62 (2015), pp. 122–145.
[9] Y. HUANG AND J. XU, *Superconvergence of quadratic finite elements on mildly structured grids*, Math. Comput., 77 (2008), pp. 1253–1268.
[10] M. K*řižek*, *Superconvergence results for linear triangular elements*, Lecture Notes in Mathematics, 1192, pp. 315-320, Springer, 1986.
[11] M. KŘIŽEK, P. NEITTAANMÄKI AND R. STENBERG, *Finite element methods: superconvergence, post-processing, and a posteriori estimates*, Lecture Notes in Pure and Applied Mathematics Series, Vol. 196, Marcel Dekker, New York, 1997.
[12] A. M. LAKHANY, I. MAREK AND J. R. WHITEMAN, *Superconvergence results in mildly structured triangulations*, Comput. Methods Appl. Mech. Engry, 189 (2000), pp. 1–75.
[13] Q. LIN AND N. YAN, The Construction and Analysis of High Efficiency Finite Elements, Hebei University Press, Hebei, China(in Chinese), 1996.
[14] P. PERSSON AND G. STRANG, *A simple mesh generator in Matlab*, SIAM Rev., 46 (2004), pp. 329–345.
[15] L. B. WAHLBIN, Superconvergence in Galkerkin Finite Element Methods, Springer Verlag, Berlin, 1995.
[16] N. Y. YI, A posteriori Error Estimates Based on Gradient Recovery and Adaptive Finite Element Methods, Ph.D. thesis, Xiangtan University, 2011.
[17] Q. ZHU, *Natural inner superconvergence for the finite element method*, (Proc. China-France Sympos. on Finite Element Methods, Beijing, 1982), Gordon and Breach, New York, pp. 935–960, 1983.
[18] Q. ZHU AND Q. LIN, Finite Element Superconvergence Theory, Hunan Science Press, Hunan, China(in Chinese), 1989.

https://doi.org/10.4208/nmtma.2017.s10 Published online by Cambridge University Press

[19] M. ZLÁMAL, *On the finite element method*, Numer. Math., 12 (1968), pp. 394–409.
[20] M. ZLÁMAL, *Superconvergence and reduced integration in the finite element method*, Math. Comput., 32 (1978), pp. 663–685.

https://doi.org/10.4208/nmtma.2017.s10 Published online by Cambridge University Press